Discrete Sources Method to solve nonlocal scattering problems in plasmonic applications

I. V. Lopushenko[1, *] **and A. G. Sveshnikov**[1, **]

[1] *Faculty of Physics, Lomonosov Moscow State University, Leninskie Gory 1/2, Moscow, 119991 Russia*

Abstract—Current paper presents a comprehensive up-to-date review of one of the most recently developed numerical schemes based on the Discrete Sources Method. The aim of these developments is to implement and justify new efficient mathematical models allowing to accurately simulate response of small plasmonic nanoparticles with scale less than 10nm to the different types of incident fields. Spatial dispersion effects of the material that are non-negligible at the given scales are incorporated into the numerical technique via Generalized Nonlocal Optical Response approach. Electron energy loss and plane wave scattering problems are considered, with the latter additionally featuring account for the presense of the substrate in the medium. Validity of the obtained results is ensured via a posteriori residual estimation, via comparison of computed scattering properties to the other available simulation techniques, and via comparison to the experimental electron energy loss measurements available in reference literature.

2010 Mathematical Subject Classification: 35Q60, 35Q90, 65N80, 78A45

Keywords and phrases: *nanoplasmonics, nonlocal effect, spatial dispersion, Maxwell equations, Discrete Sources Method*

1. INTRODUCTION

Recently a lot of attention has been devoted to problems of nanoplasmonics: a branch of science which studies unique electromagnetic properties of metal and semiconductor materials caused by collective oscillations of conductivity electrons which yield an enormous impact on modern optic and photonic applications [1].

Traditionally, interaction between such materials and electromagnetic waves can be treated mathematically using boundary-value problems for Maxwell equations, which in turn allows analytic solutions for such simple particle shapes as sphere. It gives an opportunity to understand the basic fundamentals of plasmonics, but at the same time modern technologies require precise analysis of more complex particles creating demand for advanced numerical techniques. Many fundamental works and tools exist to solve such problems, beginning with direct and universal solvers such as Finite Elements Method (FEM) or Finite Differences in Time Domain (FDTD) and finishing with numerous semi-analytical approaches that allow to vastly speed up computational performance imposing certain limitations on particle material or shape. All of the following – integral equation methods, Galerkin techniques, Discrete Dipole Approximation and various Generalized Multipole Technique implementations including Discrete Sources Method (DSM) – fall into the latter category.

Another challenge for plasmonics research and appropriate mathematical modeling emerges with the reduction of particle size below 10nm. This is due to new effects, including ones with quantum origins, which appear at these scales and which have to be accurately accounted for. One of these effects is spatial dispersion of the obstacle material which leads to nonlocal response and drastically changes scattering properties [2]. Pure quantum-based tools such as Time-Dependent Density Functional

* E-mail: lopushenko.ivan@physics.msu.ru
** E-mail: sveshnikov@phys.msu.ru

Theory (TDDFT) seem to be most appropriate instrument to study such systems, however high computational costs prevent them from being widely and effectively used. For this reason certain attempts to include nonlocality into the Maxwell boundary-value problems were made and they proved to be successful when describing properties of plasmonic systems down to 1-2nm scales [3].

Aim of the current work is to give a comprehensive up-to-date review of one of the latests developments in the semi-analytical Discrete Sources Method: a new scheme, which addresses both classic and nonlocal 3D electromagnetic scattering problems and allows to efficiently solve them using only dipole sources distibuted along particle's axis of symmetry for obstacles which size is much less than incident wavelength.

2. DISCRETE SOURCES METHOD

2.1. Method basics

Foundations of the Discrete Sources Method were laid back in the secold half of XX century by V. D. Kupradze [4]. Basic DSM principles were furtherly developed and thorougly investigated by A. G. Sveshnikov and his students, subsequently resulting both in the fully justified theory and in flexible numerical algorithms designed to efficiently solve applied electrodynamic problems [5]. In order to briefly outline these principles let us introduce notations for the simply connected bounded domain D_i with a smooth closed boundary surface ∂D_i located in the exterior domain $D_0 = \mathbb{R}^n \setminus \overline{D_i}, n \in \mathbb{N}$. Let us also introduce linear differential operator L which acts from a Hilbert space H onto itself. Also let us denote g as any compact in D_0, introduce $C(g)$ as linear space of all continuous complex-valued functions defined on g and introduce $L^2(\partial D_i)$ as Hilbert space of all square integrable functions on the ∂D_i.

The key idea is representation of the approximate solution u^δ to the exterior boundary-value problem

$$L(u) = 0 \text{ in } D_0, \tag{1a}$$

$$l(u) + l(u^0) = 0 \text{ at } \partial D_i, \tag{1b}$$

$$\text{infinity conditions} \tag{1c}$$

as a linear combination of particular solutions $\{\psi_k\}_{k=1}^{\infty}$ which form a complete closed system at ∂D_i and analytically fulfill both equation (1a) and infinity conditions. Here l is a boundary differential operator for either Dirichlet, Neumann, or impedance boundary-value problem, u is exact problem solution, and u^0 is the incident excitation field. Then, if boundary condition

$$\|l(u^\delta) + l(u^0)\| \le \delta \tag{2}$$

is approximately fullfilled in the corresponding space norm and problem (1) has a unique solution, the following estimate holds for the approximate solution [6]:

$$\|u - u^\delta\|_{C(g)} = O\Big(\|l(u^\delta) + l(u^0)\|_{L^2(\partial D_i)}\Big). \tag{3}$$

Given estimate ensures proximity of u^δ to the exact solution u in the exterior domain D_0. Therefore it is enough to approximately fullfill boundary conditions in the L^2 norm at ∂D_i surface in order to solve the original problem. This approach is generally known as quasi-solution concept. It is not limited to the exterior problems like (1) and is also valid for the interior and transmission boundary-value problems [7].

The physical interpretation of particular solution set $\{\psi_k\}$ is a set of fictitious sources which replace the particle D_i and generate the same scattered field as the actual obstacle. There are many approaches known to have similar origin including Multiple Multipole Program, fictious current models or T-Matrix Method, the difference between them being related to the type of sources used [8]. Discrete Sources Method is known to be one of the most flexible approaches which makes an efficient use of the quasi-solution concept.

In the following we will consider electromagnetic scattering problems with L representing a Maxwell system. Within DSM a set of the corresponding particular solutions can be represented as a set of

linearly independent solutions to Helmholtz equation for the vector potential $\mathbf{A}$ of the electromagnetic field:

$$(\Delta + k_\zeta^2)\mathbf{A} = 0 \text{ in } D_\zeta, \zeta = 0, i. \tag{4}$$

Here $k_\zeta^2 = (2\pi/\lambda)^2\varepsilon_\zeta\mu_\zeta = (\omega/c)^2\varepsilon_\zeta\mu_\zeta$ is a wave number in the corresponding domain D_ζ . Values λ, ω, c and $\varepsilon_\zeta, \mu_\zeta$ are also intoduced for the wavelength, angular frequency, speed of light in vacuum and freqiency dependent material permittivities, respectively. For the scattered field this set of solutions usually represents a system of discrete fictitious radiating multipoles with unknown amplitudes. It is important to note that discrete sources (DS) system should be complete in $L^2(\partial D_i)$. Most widely used examples are the system of electric dipoles distributed over an auxiliary surface $S \subset D_i$ and the system of electric and magnetic multipoles distributed along the axis of symmetry of the particle [8]. As a rule, support of the DS set becomes more complicated with the simplification of the DS field form, and vice versa.

Within the imposed constraints both form and location of the discrete sources can be adjusted to provide the best match to the specific problem conditions. For example, construction of the DS fields using Green Tensor of the layered medium allows to analytically satisfy the boundary conditions on the infinite medium interface along with the Maxwell equations and to rigorously solve corresponding scattering problems. Another example is the choice of electric and magnetic multipoles with support on the axis for the axisymmetric problems. In this case the original problem is reduced to a set of one-dimensional problems for matching each Fourier harmonic of the incident field to the corresponding multipole fields at the particle generatrix which ensures very high performance of the computer implementation [8]. For particles with non-axisymmetric shapes dipole sources with the auxiliary surface support and boundary conditions matching at the whole particle surface ∂D_i are usually used.

2.2. Small obstacle problems

However, recently usage of the adverted DS systems has proved to be rebundant in some problems, particularly related to the field of nanoplasmonics featuring extremely small-scaled particles. Namely, in the case of optical plane wave (PW) scattering by axisymmetric particle with size less than 10nm it is enough to account only for the first harmonics of the corresponding PW Fourier expansion, making possible to use only electric and magnetic dipole sources on the obstacle axis. Let us elaborate on this statement. Firstly, let us show that for the given obstacle scale first harmonics form a main contribution to the PW field. Indeed,

$$\exp(\pm j\nu\cos\phi) = \sum_{m=0}^{\infty}(2-\delta_{0m})(\pm j)^m J_m(\nu)\cos(m\phi) \tag{5}$$

stands for the expansion of the plane wave exponential term, where $J_m(\cdot)$ is a Bessel function of the first kind of order m and j is the imaginary unit. In order to strictly define ν let us consider an axisymmetric obstacle D_i and introduce Cartesian coordinate system with z axis coinciding with the axis of symmetry. Let us also assume that particle maximum size along the x or y axis is denoted as a. We would subsequently consider a as transverse radius of the particle. In the following we would also assume that particle maximum size in both x and y dimensions is the same without the loss of generality. Let us also introduce spherical $\{r, \theta, \varphi\}$ and cylindrical $\{r, \varphi, z\}$ coordinate systems corresponding to the introduced Cartesian coordinates. Then, using expressions for P-polarized plane wave in $\exp(j\omega t)$ time dependence

$$\begin{aligned}\mathbf{E}_0^{0,P}(M) &= (\mathbf{e}_x\cos\theta_0 + \mathbf{e}_z\sin\theta_0)\cdot\exp\left\{-jk_0\left(x\sin\theta_0 - z\cos\theta_0\right)\right\},\\ \mathbf{H}_0^{0,P}(M) &= -\mathbf{e}_y\cdot n_0\cdot\exp\left\{-jk_0\left(x\sin\theta_0 - z\cos\theta_0\right)\right\}\end{aligned} \tag{6}$$

for a wave propagating at angle $\pi - \theta_0$ to axis z we arrive at maximum possible value $\nu_{max} = k_0 a$ assuming that $\theta_0 = \pi/2$. Here $n_0^2 = \varepsilon_0\mu_0$. As soon as (5) represents an alternating series we can use last discarded term to estimate the contribution of the first several terms:

$$\frac{2J_1(k_0a)}{J_0(k_0a)} \le \delta_0, \quad \frac{2J_2(k_0a)}{|J_0(k_0a) - 2jJ_1(k_0a)|} \le \delta_1, \tag{7}$$

where δ_m refers to the specified approximation accuracy of the first m terms. Assuming $\delta_0 = 10\%$, and $\lambda = 532$nm corresponding to the optical wavelength range, we arrive at scale estimate $a \leq 8$nm. At the same time $\delta_1 = 0.2\%$. Various estimates for the other wavelengths retaining values for $\delta_{0,1}$ are presented in the table 1. It is important to note that these limitations are not imposed on the particle size along the z axis which could therefore be larger than a without loss of accuracy.

Table 1. Estimate of the particle transverse radius a at which it is sufficient to account only for the first term of the plane wave expansion

λ, nm	100	200	300	400	500	600	700	800	900
a, nm	1.59	3.2	4.77	6.36	7.94	9.54	11.13	12.72	14.31

Now let us follow the general DSM computational scheme for electromagnetic scattering problems. We would like to study properties of dipole discrete source sets. Single radiating dipoles are constructed as fundamental solutions to (4):

$$\psi(M, M_n) = \exp(-jk_0 R_{MM_n})/R_{MM_n}, \quad \mathbf{A}_l(M, M_n) = \psi(M, M_n)\mathbf{e}_l. \tag{8}$$

Here $M = M(x, y, z)$ is a point of field computation, point $M_n = M_n(x_n, y_n, z_n)$ corresponds to the source location which will be defined later, $R^2_{MM_n} = (x - x_n)^2 + (y - y_n)^2 + (z - z_n)^2$ and $\mathbf{e}_l$ is an arbitrary unit vector collinear to the dipole moment. In the following l index will be used to denote the direction of this vector, i.e. $\mathbf{e}_x$ corresponds to the ort of the introduced Cartesian system. An alternative convenient way to write down fundamental solution is $h_0^{(2)}(k_0 R_{MM_n})$ which is obviously the same as $\psi(M, M_n)$ up to a constant factor. Here $h_0^{(2)}(\cdot)$ corresponds to a zero-order spherical Hankel function of the second kind, which satisfies infinity conditions in the selected time dependence $\exp(j\omega t)$. We can then write down fields for the electric 'e' and magnetic 'h' discrete sources in the exterior domain as

$$\begin{aligned}
&\mathbf{E}^e_{0,l}(M, M_n) = \frac{j}{k\varepsilon_0\mu_0}\,\mathrm{curlcurl}\mathbf{A}_l(M, M_n), \;\; \mathbf{H}^e_{0,l}(M, M_n) = -\frac{1}{\mu_0}\,\mathrm{curl}\mathbf{A}_l(M, M_n),\\
&\mathbf{E}^h_{0,l}(M, M_n) = \frac{1}{\varepsilon_0}\,\mathrm{curl}\mathbf{A}_l(M, M_n), \;\; \mathbf{H}^h_{0,l}(M, M_n) = \frac{j}{k\varepsilon_0\mu_0}\,\mathrm{curlcurl}\mathbf{A}_l(M, M_n).
\end{aligned} \tag{9}$$

Here $k = 2\pi/\lambda$. The following statement allows to employ electric and magnetic dipole discrete sources deposited on the auxiliary surface inside the particle to rigorously solve the exterior scattering problem for Maxwell equatuions by particle with any smooth boundary including axisymmetric ones [9]:

Theorem 1. *Let $S \subset D_i$ be an auxiliary cylindrical surface of radius ρ_S which axis coincides with axis z of the Cartesian coordinate system, and let $\overline{\{M_n\}}_{n=1}^{\infty} = S$. Let us assume that electric and magnetic dipoles are located in each of $M_n \in S$ and their dipole monents are oriented along vectors $\mathbf{v}_1(M_n), \mathbf{v}_2(M_n)$ tangential to S and orthogonal both to each other and to unit outward normal at M_n. Then resulting systems of vector functions (9) are complete and closed in $L^2_\tau(\partial D_i)$.*

Here we introduced $L^2_\tau(\partial D_i)$ space of square integrable tangential fields which is clearly a subspace of $L^2(\partial D_i)$. We would furtherly suggest that we investigate axisymmetric particles, and that axis O_z of the introduced Cartesian system coincides with obstacle axis in this section. Now let us investigate a specific case of dipole sources being distributed along the particle axis. Assuming $\rho_S \to 0$ and using the addition theorem

$$\psi(M, P) = -jk \sum_{i=0}^{\infty} \sum_{m=-i}^{i} \left(N_{im} j_i(kR_P) P_i^m(\cos\theta_P) h_i^{(2)}(kR_M) P_i^m(\cos\theta_M) e^{jm(\phi_M - \phi_P)} \right) \tag{10}$$

it can be easily shown that $P_i^m(\cos\theta_M) \overset{\rho_S\to 0}{\longrightarrow} P_i^m(1)$ which equals to zero in case of $m > 0$ and therefore only first term of PW expansion (5) can be approximated by the given DS set. Here $M \in \partial D_i$, $P \in S$, $j_i(\cdot)$ – spherical Bessel functions, $P_i^m(\cdot)$ – associated Legendre polynomials, $N_{im}^2 = (2i+1)(i-|m|)/(4\pi(i+|m|))$, $\theta_{M,P}$ and $\varphi_{M,P}$ – spherical coordinates of M and P.

Finally, it is necessary to outline statements that ensure completeness of the dipole discrete sources deposited on the particle axis of symmetry and oriented along orts of the Cartesian coordinate system for the fields of specific structure featuring only first Fourier harmonics.

Theorem 2. *Let all restrictions imposed earlier on ∂D_i, D_i and D_0 be satisfied. Let us consider a bounded sequence$(z_n) \subset \Gamma_z$, where Γ_z is a segment of the z-axis inside D_i, and let $\{z_n\}_{n=1}^{\infty}$ to have at least one accumulation point. Then system*

$$\mathbf{E}_{0,z}^e(M, z_n) = \frac{j}{k\varepsilon_0\mu_0}\mathrm{curlcurl}\{h_0^{(2)}(k_0 R_{Mz_n})\mathbf{e}_z\} \tag{11}$$

is complete in $L_\tau^2(\partial D_i)$ for elements of this space that do not depend on any azimuthal mode φ.

This result allows to use the so-called 'vertical' dipoles oriented along $\mathbf{e}_z$ to approximate fields that do not depend on the azimutal angle φ [10]. The following statement, in turn, allows to compose a complete system for the first Fourier harmonic [8]:

Theorem 3. *Let us consider conditions of Theorem 2. Then system*

$$\mathbf{E}_{0,x}^{e,h}(M, z_n),\ \mathbf{E}_{0,y}^{e,h}(M, z_n),\ \mathbf{H}_{0,x}^{e,h}(M, z_n),\ \mathbf{H}_{0,y}^{e,h}(M, z_n) \tag{12}$$

is complete in $L_\tau^2(\partial D_i)$ for elements that depend on first azimuthal mode φ.

To summarize, if the incident electromagnetic wave field can be efficiently described by the terms either not depending on azimuthal angle φ or depending as $\cos\varphi$ or $\sin\varphi$, then usage of general DSM schemes is rebundant to solve the problem and it is possible to use only dipole sources on the axis of symmetry of the obstacle to investigate scattering properties. It is also important to note that this approach allows to satisfy boundary conditions on the particle surface ∂D_i both via Fourier harmonic matching on the particle generatrix and via total field matching on the whole surface, with latter being of special interest due to the possibility of analyzing wider scope of problems.

These statements form concept of the new DSM scheme which is called hybrid. For practical applications it is important that any fields with named specific feature of main contribution made by the first Fourier harmonics can be approximated by the set (12) of discrete sources. Besides plane waves this also stands true, for example, for the fields generated by fast relativistic electrons used in the electron energy loss spectroscopy (EELS). Therefore hybrid DSM scheme allows to solve given size- and field-specific scattering problems using a narrower class of complete and closed set of linearly independent DS along with the simple structure of the DS support. In the following these results will be confirmed by the numerical experiments.

3. 3D SCATTERING PROBLEMS WITHOUT ACCOUNT FOR SPATIAL DISPERSION

3.1. Problem statement

In order to outline the numerical algorithm of the hybrid DSM let us first consider electromagnetic scattering by transparent obstacles deposited either on a substrate or in free space without account for possible material spatial dispersion effects. In order to do so let us assume that exterior medium consists of two homogeneous layers split by plane interface Σ and that particle D_i is fully deposited in the upper halfspace domain D_0. Substrate domain is then denoted as D_1. For convenience reasons let us introduce a new Cartesian coordinate system with $z = 0$ at Σ, and corresponding cylindrical and

spherical coordinates with the same origin retaining notations from the previous section. Then problem statement takes the following form:

$$\mathrm{curl}\mathbf{H}_i(M) = jk\varepsilon_T\mathbf{E}_i(M), \tag{13a}$$
$$\mathrm{curl}\mathbf{E}_i(M) = -jk\mu_i\mathbf{H}_i(M) \quad \text{in} \quad D_i, \tag{13b}$$

$$\mathrm{curl}\mathbf{H}_\zeta(M) = jk\varepsilon_\zeta\mathbf{E}_\zeta(M), \tag{13c}$$
$$\mathrm{curl}\mathbf{E}_\zeta(M) = -jk\mu_\zeta\mathbf{H}_\zeta(M) \quad \text{in} \quad D_\zeta, \quad \zeta = 0,1, \tag{13d}$$

$$\mathbf{E}_0(M) = \mathbf{E}_0^S(M) + \mathbf{E}_0^0(M), \tag{13e}$$
$$\mathbf{E}_1(M) = \mathbf{E}_1^S(M) + \mathbf{E}_1^0(M), \tag{13f}$$

$$\hat{\mathbf{n}}_P \times (\mathbf{E}_i(P) - \mathbf{E}_0(P)) = 0, \tag{13g}$$
$$\hat{\mathbf{n}}_P \times (\mathbf{H}_i(P) - \mathbf{H}_0(P)) = 0, \quad P \in \partial D_i, \tag{13h}$$

$$\mathbf{e}_z \times (\mathbf{E}_0(Q) - \mathbf{E}_1(Q)) = 0, \tag{13i}$$
$$\mathbf{e}_z \times (\mathbf{H}_0(Q) - \mathbf{H}_1(Q)) = 0, \quad Q \in \Sigma, \tag{13j}$$

$$\lim_{r\to\infty} r \cdot (\sqrt{\varepsilon_0}\,\mathbf{E}_0^S \times \frac{\mathbf{r}}{r} - \sqrt{\mu_0}\,\mathbf{H}_0^S) = 0, \quad r = |M| \to \infty, \quad z > 0, \tag{13k}$$
$$(|\mathbf{E}_1^S|, |\mathbf{H}_1^S|) = o(\exp\{-|\mathrm{Im}k_1|r\}), \quad z < 0. \tag{13l}$$

Most importantly, here we explicitly emphasize that material complex dielectric permittivity is denoted as ε_T in order to comply with notations of the next section. Also here $\varepsilon_{0,1}, \mu_{0,1}$ are material parameters of $D_{0,1}$ domains, $\{\mathbf{E}_\zeta, \mathbf{H}_\zeta\}$ is total electromagnetic field in the domain D_ζ, $\zeta = \{0,1,i\}$, $\{\mathbf{E}_\zeta^S, \mathbf{H}_\zeta^S\}$ denotes the scattered field, $\{\mathbf{E}_\zeta^0, \mathbf{H}_\zeta^0\}$ denotes the excitation field, $\hat{\mathbf{n}}_P$ represents a unit outward normal to the particle surface ∂D_i at point $P \in \partial D_i$ and the following relations are satisfied: $\mathrm{Im}\varepsilon_0, \mu_0 = 0, \mathrm{Im}\varepsilon_{1,T}, \mu_1 < 0$. Under given conditions problem (13) has a unique solution.

In the following we would consider P-polarized plane wave fields for both the layered medium and free space problems without the loss of generality, as S-polarized waves are treated identically. Excitation field for the P-wave is written similar to (6):

$$\begin{aligned}
&\mathbf{E}_0^{0(P)} = \mathbf{E}_0^{0,P(-)} + R_P \cdot \mathbf{E}_0^{0,P(+)}, \quad z \geq 0,\\
&\mathbf{H}_0^{0(P)} = \mathbf{H}_0^{0,P(-)} + R_P \cdot \mathbf{H}_0^{0,P(+)}, \quad z \geq 0,\\
&\mathbf{E}_{0,\zeta}^{P(\pm)} = (\mp\mathbf{e}_x \cos\theta_\zeta \cos\varphi_t \mp \mathbf{e}_y \cos\theta_\zeta \sin\varphi_t + \mathbf{e}_z \sin\theta_\zeta) \cdot \gamma_\zeta^{(\pm)},\\
&\mathbf{H}_{0,\zeta}^{P(\pm)} = (\mathbf{e}_x \sin\varphi_t - \mathbf{e}_y \cos\varphi_t) \cdot n_\zeta \cdot \gamma_\zeta^{(\pm)}.
\end{aligned} \tag{14}$$

Here $\gamma_\zeta^{(\pm)} = \exp\{-jk_\zeta\,(x\sin\theta_\zeta\cos\varphi_t + y\sin\theta_\zeta\sin\varphi_t \pm z\cos\theta_\zeta)\}$, $n_\zeta^2 = \varepsilon_\zeta\mu_\zeta$, and

$$R_P = \frac{n_1\cos\theta_0 - n_0\cos\theta_1}{n_1\cos\theta_0 + n_0\cos\theta_1}, \quad R_S = \frac{n_0\cos\theta_0 - n_1\cos\theta_1}{n_0\cos\theta_0 + n_1\cos\theta_1}.$$

Also explicitly for the free space scattering problem we would consider an additional external excitation field of a fast electron [3]:

$$\begin{aligned}
&\mathbf{E}_{0,x}^0 = \frac{x-b_x}{\rho}\frac{2e\omega}{v^2\gamma_1}e^{i\omega\frac{z}{v}}K_1(\frac{\omega\rho}{v\gamma_1}), && \mathbf{H}_{0,x}^0 = -\frac{y-b_y}{\rho}\frac{2e\omega}{v\gamma_1}e^{i\omega\frac{z}{v}}K_1(\frac{\omega\rho}{v\gamma_1}),\\
&\mathbf{E}_{0,y}^0 = \frac{y-b_y}{\rho}\frac{2e\omega}{v^2\gamma_1}e^{i\omega\frac{z}{v}}K_1(\frac{\omega\rho}{v\gamma_1}), && \mathbf{H}_{0,y}^0 = \frac{x-b_x}{\rho}\frac{2e\omega}{v\gamma_1}e^{i\omega\frac{z}{v}}K_1(\frac{\omega\rho}{v\gamma_1}),\\
&\mathbf{E}_{0,z}^0 = \frac{i}{\gamma_1^2}\frac{2e\omega}{v^2\gamma_1\varepsilon}e^{i\omega\frac{z}{v}}K_0(\frac{\omega\rho}{v\gamma_1}), && \mathbf{H}_{0,z}^0 = 0.
\end{aligned} \tag{15}$$

Here we assume that electron is represented as a point charge in uniform motion along z axis and its trajectory does not cross particle border ∂D_i. Distance of electron trajectory from the origin of coordinate system is defined by the impact factor $\mathbf{b} = \{b_x, b_y\}$. Also here $\rho^2 = (x - b_x)^2 + (y - b_y)^2$, $K_n(\cdot)$ is a modified Bessel function of the second kind and order n, v is electron speed, $\gamma_1 = \left(\sqrt{1 - v^2/c^2}\right)^{-1}$ is Lorentz factor and $e = -4.8 \cdot 10^{-10}$Fr is elementary charge. These fields also comply with the restrictions of the hybrid DSM scheme discussed in section 2.2.

3.2. Computational algorithm

3.2.1. Discrete Sources for the internal field In order to solve the scattering problem we need to write down the solution for the interior problem in the D_i domain first. It is constructed similarly to the solution in the homogeneous exterior domain D_0 following the procedure described in section 2.2. The only difference is that we would use another fundamental solution to the equation (4) in the form $\psi_{int}(M, M_n) = \sin(k_i R_{MM_n})/R_{MM_n}$ that does not have singularity inside D_i and that does not have to meet radiation conditions. The alternative way to write down this solution is to introduce spherical Bessel functions of zero order $j_0(k_i R_{MM_n})$. These DS can be deposited inside the particle on the axis of symmetry and their fields can be computed from (9) substituting relevant material permittivities ε_T, μ_i instead of ε_0, μ_0 and vector potential with the new fundamental solution ψ_{int}.

Knowing the DS fields, we can now construct the approximate solution to the interior problem:

$$\begin{aligned}
\mathbf{E}_i^N(M) &= \sum_{n=1}^{N} \sum_{\alpha=x,y,z} \Big(p_{\alpha,n}^T \mathbf{E}_{T,\alpha}^e(M, M_n) + q_{\alpha,n}^T \mathbf{E}_{T,\alpha}^h(M, M_n) \Big), \\
\mathbf{H}_i^N(M) &= \sum_{n=1}^{N} \sum_{\alpha=x,y,z} \Big(p_{\alpha,n}^T \mathbf{H}_{i,\alpha}^e(M, M_n) + q_{\alpha,n}^T \mathbf{H}_{i,\alpha}^h(M, M_n) \Big).
\end{aligned} \tag{16}$$

Here we assume that three electric discrete sources and three magnetic discrete sources, each of them oriented along one of orts of the Cartesian coordinate system, are deposited in $\{M_n\}_{n=1}^N$ points distributed over the particle axis of symmetry. $p_{\alpha,n}^T$ are amplitudes of the electric sources in the n-th point, and $q_{\alpha,n}^T$ are amplitudes of the corresponding magnetic sources. Index T emphasizes the fact that all considered here electromagnetic fields are transversal, which is an important detail.

3.2.2. Discrete Sources for the scattered field In order to construct solution for the exterior problem with account for substrate presence we would require Green Tensor of the layered medium [11]:

$$\widehat{\mathbf{G}}^{e,h}(M, M_n) = \begin{bmatrix} G^{e,h} & 0 & 0 \\ 0 & G^{e,h} & 0 \\ \partial g^{e,h}/\partial x_M & \partial g^{e,h}/\partial y_M & G^{h,e} \end{bmatrix}.$$

Tensor components are expressed in the form of Sommerfeld integrals and allow to analytically take into account interaction with the substrate:

$$G^{e,h}(M, M_n) = \int_0^\infty J_0(\lambda r) \nu_{11}^{e,h}(\lambda, z, z_n) \lambda \, d\lambda, \quad g^{e,h}(M, M_n) = \int_0^\infty J_0(\lambda r) \nu_{31}^{e,h}(\lambda, z, z_n) \lambda \, d\lambda.$$

Here $r^2 = (x - x_n)^2 + (y - y_n)^2$, $R_{MM_n}^2 = r^2 + (z - z_n)^2$, '$e$' and '$h$' correspond to the components of electric and magnetic tensor types, correspondingly. Spectral functions $\nu_{11}^{e,h}, \nu_{31}^{e,h}$ with factors $A_{mn}^{e,h}, B_{mn}^{e,h}$ are determined from the conditions imposed on the interface Σ and analytically ensure their validity:

$$\nu_{11}^{e,h}(\lambda, z, z_n) = \begin{cases} \dfrac{\exp(-\eta_0 |z - z_n|)}{\eta_0} + A_{11}^{e,h}(\lambda, z_n) \cdot \exp(-\eta_0 z), & z_n > 0, \ z \geq 0, \\ B_{11}^{e,h}(\lambda, z_n) \cdot \exp(\eta_1 z), & z_n > 0, \ z \leq 0, \end{cases}$$

$$\nu_{31}^{e,h}(\lambda,z,z_n)=\begin{cases}A_{31}^{e,h}(\lambda,z_n)\cdot\exp(-\eta_0 z), & z_n>0,\ z\geq 0,\\ B_{31}^{e,h}(\lambda,z_n)\cdot\exp(\eta_1 z), & z_n>0,\ z\leq 0.\end{cases}$$

$$A_{11}^{e,h}(\lambda,z_n)=\frac{\chi_0^{e,h}-\chi_1^{e,h}}{\chi_0^{e,h}+\chi_1^{e,h}}\cdot\frac{\exp(-\eta_0 z_n)}{\eta_0},\quad B_{11}^{e,h}(\lambda,z_n)=\frac{2\chi_0^{e,h}}{\chi_0^{e,h}+\chi_1^{e,h}}\cdot\frac{\exp(-\eta_0 z_n)}{\eta_0},$$

$$A_{31}^{e,h}(\lambda,z_n)=\frac{2\kappa\cdot\exp(-\eta_0 z_n)}{(\chi_0^{e}+\chi_1^{e})(\chi_0^{h}+\chi_1^{h})},\qquad B_{31}^{e,h}(\lambda,z_n)=\Big(\frac{\mu_1}{\mu_0},\frac{\varepsilon_1}{\varepsilon_0}\Big)\frac{2\kappa\cdot\exp(-\eta_0 z_n)}{(\chi_0^{e}+\chi_1^{e})(\chi_0^{h}+\chi_1^{h})},$$

Here $\eta_\zeta^2=\lambda^2-k_\zeta^2$, $\chi_\zeta^e=\eta_\zeta/\mu_\zeta$, $\chi_\zeta^h=\eta_\zeta/\varepsilon_\zeta$, $\kappa=(\varepsilon_0\mu_0)^{-1}-(\varepsilon_1\mu_1)^{-1}$. Let us note that we consider particle fully embedded in the upper halfspace D_0, so we would omit expressions related to the sources with $z_n<0$. Now we can write down new expressions for the vector potentials of the exterior discrete sources:

$$\mathbf{A}_{x,n}^{e,h}=G^{e,h}\mathbf{e}_x+\partial g^{e,h}/\partial x_M\mathbf{e}_z,\quad \mathbf{A}_{y,n}^{e,h}=G^{e,h}\mathbf{e}_y+\partial g^{e,h}/\partial x_M\mathbf{e}_z,\quad \mathbf{A}_{z,n}^{e,h}=G^{h,e}\mathbf{e}_z. \tag{17}$$

Fields of these DS can be obtained from (9) substituting vector potentials expressed via Green Tensor components. Then approximate solution for the scattered field in D_0 domain is constructed as:

$$\mathbf{E}_0^{S,N}(M)=\sum_{n=1}^{N}\sum_{\alpha=x,y,z}\Big(p_{\alpha,n}^0\mathbf{E}_{0,\alpha}^e(M,M_n)+q_{\alpha,n}^0\mathbf{E}_{0,\alpha}^h(M,M_n)\Big),$$

$$\mathbf{H}_0^{S,N}(M)=\sum_{n=1}^{N}\sum_{\alpha=x,y,z}\Big(p_{\alpha,n}^0\mathbf{H}_{0,\alpha}^e(M,M_n)+q_{\alpha,n}^0\mathbf{H}_{0,\alpha}^h(M,M_n)\Big). \tag{18}$$

Similarly to the interior problem solution we assume that three electric DS and three magnetic DS are deposited in $\{M_n\}_{n=1}^N$ set of points distributed over the particle axis of symmetry. Let us note that generally sets for interior sources $\{M_n\}_{n=1}^{N_{int}}$ and for the exterior sources $\{M_n\}_{n=1}^{N_{ext}}$ could be either different ($N_{int}\neq N_{ext}$) or could be one and the same set ($N_{int}=N_{ext}=N$). In the following we would use one set of points for the simplicity reasons and without any loss of generality. We also retain notations p,q for the unknown DS amplitudes changing the upper index to 0 according to D_0 domain. It should be noted that in the case of $\varepsilon_0=\varepsilon_1,\mu_0=\mu_1$ vector potentials (17) are reduced to their free space counterparts (8) as follows from performing Sommerfeld integration after substituting material parameters into expressions for spectral coefficients.

3.2.3. Expessions for the most common scattering properties within DSM In order to investigate experimentally measurable properties of the particles and particle systems it is necessary to compute scattering characteristics in addition to the construction of approximate solution. For this purpose we would employ radiation pattern in the far zone $\mathbf{F}$ which is defined as

$$\frac{\mathbf{E}_\zeta^S(M)}{\Big|\mathbf{E}_\zeta^0(M)\Big|}=\frac{\exp\{-jk_\zeta R\}}{R}\mathbf{F}^\zeta(\theta,\theta_0,\varphi)+O(1/R^2),R=|M|\to\infty,M\in D_\zeta. \tag{19}$$

One of the DSM advantages is that it allows to express components of $\mathbf{F}$ analytically in the form of linear combination of elementary functions even for the scattering problems in the layered medium. This is achieved via asymptotic estimation of Sommerfeld integrals in the far zone via stationary-phase method:

$$\overline{G}^{e,h}(M,M_n)=|\cos\theta|\cdot\exp\Big(jk_\zeta\sin\theta(x_n\cos\varphi+y_n\sin\varphi)\Big)\cdot\nu_{11}^{e,h}(k_\zeta\sin\theta,z=0,z_n)$$

$$\overline{g}^{e,h}(M,M_n)=|\cos\theta|\cdot\exp\Big(jk_\zeta\sin\theta(x_n\cos\varphi+y_n\sin\varphi)\Big)\cdot\nu_{31}^{e,h}(k_\zeta\sin\theta,z=0,z_n) \tag{20}$$

Here it might seem that there appears to be a singularity at $\eta_0=0$ due to the explicit expression for spectral function ν_{11}. However it can be clearly seen that for the particle located in the upper half-space $z_n>0$ exponential term $\exp(-\eta_0 z_n)$ in ν_{11} can be factored out and fractions could be reduced to a

common denominator eliminating possible singularity. Then the following stands for $\mathbf{F}^\zeta = \{F_R^\zeta, F_\theta^\zeta, F_\varphi^\zeta\}$ within hybrid DSM scheme:

$$\begin{aligned}
F_\theta^\zeta(\theta,\theta_0,\varphi) = \quad & k^2 \sum_{n=1}^{N^\zeta} \Big\{ p_{x,n}^0 \cos\varphi \left(-\varepsilon_\zeta^{\frac{1}{2}} \mu_\zeta^{\frac{1}{2}} \cos\theta \cdot \overline{G}^e - j \sin^2\theta \cdot k \varepsilon_\zeta \mu_\zeta \overline{g}^e \right) + \\
& + p_{y,n}^0 \sin\varphi \left(-\varepsilon_\zeta^{\frac{1}{2}} \mu_\zeta^{\frac{1}{2}} \cos\theta \cdot \overline{G}^e - j \sin^2\theta \cdot k \varepsilon_\zeta \mu_\zeta \overline{g}^e \right) + \\
& + p_{z,n}^0 \left(\varepsilon_\zeta^{\frac{1}{2}} \mu_\zeta^{\frac{1}{2}} \sin\theta \cdot \overline{G}^h \right) + q_{x,n}^0 \sin\varphi \left(\mu_\zeta \overline{G}^h \right) + q_{y,n}^0 \cos\varphi \left(-\mu_\zeta \overline{G}^h \right) \Big\} \\
F_\varphi^\zeta(\theta,\theta_0,\varphi) = \quad & k^2 \sum_{n=1}^{N^\zeta} \Big\{ p_{x,n}^0 \sin\varphi \left(\varepsilon_\zeta^{\frac{1}{2}} \mu_\zeta^{\frac{1}{2}} \overline{G}^e \right) + p_{y,n}^0 \cos\varphi \left(-\varepsilon_\zeta^{\frac{1}{2}} \mu_\zeta^{\frac{1}{2}} \overline{G}^e \right) + \\
& + q_{x,n}^0 \cos\varphi \left(\mu_\zeta \cos\theta \cdot \overline{G}^h + \sin^2\theta \cdot jk \varepsilon_\zeta^{\frac{1}{2}} \mu_\zeta^{\frac{3}{2}} \overline{g}^h \right) + \\
& + q_{y,n}^0 \sin\varphi \left(\mu_\zeta \cos\theta \cdot \overline{G}^h + \sin^2\theta \cdot jk \varepsilon_\zeta^{\frac{1}{2}} \mu_\zeta^{\frac{3}{2}} \overline{g}^h \right) + q_{z,n}^0 \left(-\mu_\zeta \sin\theta \cdot \overline{G}^e \right) \Big\} \qquad (21)
\end{aligned}$$

Expression for F_R^ζ is omitted because it is equal to zero. Obtained formulas do not include Sommerfeld integration procedures and therefore ensure high computational performance. Based on these expressions we can also compute differential scattering cross-section (DSC) and total scattered field intensity σ, which we would also denote as scattering cross-section (SCS):

$$I^\zeta(\theta,\theta_0,\varphi) = \left| F_\theta^\zeta(\theta,\theta_0,\varphi) \right|^2 + \left| F_\varphi^\zeta(\theta,\theta_0,\varphi) \right|^2. \qquad (22)$$

$$DSC(\theta,\theta_0,\varphi) = I^0(\theta,\theta_0,\varphi), \quad \sigma(\theta_0) = \int_\Omega \mathrm{DSC}(\theta_0,\theta,\varphi) d\Omega. \qquad (23)$$

Here Ω is a unit sphere in the case of free space problem, and a unit hemisphere in the upper halfspace D_0 not crossing Σ in the case of problem with the substrate. It is also important to note that identical layer parameters $\varepsilon_0 = \varepsilon_1, \mu_0 = \mu_1$ easily lead to the reduction of expressions (21) to their free space equivalents.

For the EELS problems we would employ an expression for the electron energy loss probability [3]:

$$P(\omega) = \frac{e}{\pi\hbar\omega} \int_{-\infty}^{+\infty} \mathrm{Re}\left\{ \mathbf{E}_0^{S,N}(\mathbf{r}_e,\omega) e^{-i\omega z/v} \right\} d\mathbf{r}_e. \qquad (24)$$

Here $\mathbf{r_e}$ is the electron position and $\hbar$ is the reduced Planck constant. Let us note that analytic expressions for the scattered field featured in DSM allow to simplify the integral computation. One of the means to perform evaluation of (24) is to use vectorized adaptive quadrature formulas [12].

3.2.4. Overdetermined system of equations In order to compute the above scattering properties it is required to implement a numerical procedure which would deposit discrete sources on the particle axis, compute their fields along with incident fields and match the boundary conditions on the ∂D_i.

In this paper we would distribute DS uniformly along the particle axis and contain them inside the particle. To match boundary conditions we would employ generalized point matching technique. The main difference from the general DSM scheme for axisymmetric particles is that we would not distribute matching points over the particle generatrix matching Fourier harmonics of the fields at the boundary. Instead, we would distribute matching points all over the particle surface and match field values at the boundary in the same way it is done for the non-axisymmetric particles in the general scheme. This approach generally could require more computational resources, but at the same time it would allow to

consider multiple particle configurations such as dimers which do not form an axisymmetric system, for example when several particles are deposited on the substrate or have different sizes. Also this approach would generally confirm the applicability of the hybrid scheme to a wide scope of scattering problems.

Following the described procedure, let us introduce set of matching points $\{P_l\}_{l=1}^K$ uniformly distributed over surface ∂D_i. Then at each matching point we would write down boundary conditions in the following form:

$$\begin{aligned}
\left(\mathbf{E}_i^N(P_l) - \mathbf{E}_0^{S,N}(P_l)\right) \cdot \hat{\tau}_{P_l} &= \mathbf{E}_0^0(P_l) \cdot \hat{\tau}_{P_l}, \\
\left(\mathbf{E}_i^N(P_l) - \mathbf{E}_0^{S,N}(P_l)\right) \cdot \hat{\mathbf{t}}_{P_l} &= \mathbf{E}_0^0(P_l) \cdot \hat{\mathbf{t}}_{P_l}, \\
\left(\mathbf{H}_i^N(P_l) - \mathbf{H}_0^{S,N}(P_l)\right) \cdot \hat{\tau}_{P_l} &= \mathbf{H}_0^0(P_l) \cdot \hat{\tau}_{P_l}, \\
\left(\mathbf{H}_i^N(P_l) - \mathbf{H}_0^{S,N}(P_l)\right) \cdot \hat{\mathbf{t}}_{P_l} &= \hat{\mathbf{H}}_0^0(P_l) \cdot \hat{\mathbf{t}}_{P_l}.
\end{aligned} \tag{25}$$

Here $\hat{\tau}_{P_l}, \hat{\mathbf{t}}_{P_l}$ are unit vectors tangential to the surface at P_l and orthogonal both to each other and to unit outward normal at the same point. Unknowns in this system of linear equations are amplitudes of discrete sources: $\left\{p_{\alpha,n}^T, p_{\alpha,n}^0, q_{\alpha,n}^T, q_{\alpha,n}^0\right\}_{n=1}^N$. In the course of previous research on the Discrete Sources Method it has been determined that most stable results can be obtained with the pseudoinversion of overdetermined system of equations in the l_2 norm, when the number of matching points is greater than number of unknown amplitudes: $K > 12N$. For problems with the substrate it is usually required to employ Tikhonov regularization algorithm in order to efficiently perform corresponding inversion [5]. Another useful criteria is to distribute matching points on the boundary with enough density, with intervals between neighboring pairs of points being far less than the wavelength, and to distribute discrete sources neither too near nor too far from the particle boundary in order to obtain well-conditioned matrix [8].

Let us say a few more words about scattering problems with the substrate. As opposed to the free space problems with $\varepsilon_0 = \varepsilon_1, \mu_0 = \mu_1$, it is required to numerically compute Sommerfeld integrals in order to obtain DS fields via Green Tensor components $G^{e,h}, g^{e,h}$. For this purpose in the current paper we employ a highly efficient double-exponential transformation technique [13].

Key advantage of using DSM with the generalized matching point technique is the ability to perform an a-posteriori error estimation. Within the proposed hybrid scheme it can be described as follows. In addition to the matching point set $\{P_l\}_{l=1}^K$ we introduce another set $\{B_l\}_{l=1}^Q \in \partial D_i$, $\{P_l\} \cap \{B_l\} = \varnothing$. Then error estimate is computed via substitution of the approximate solution obtained with $\{P_l\}_{l=1}^K$ set into a boundary system composed in the same way for the $\{B_l\}_{l=1}^Q$ set and determination of the system residual in l_2 norm. With the DS amplitudes determined, the scattering problem is solved and it is possible to compute both electromagnetic fields and the required system properties featured above in section 3.2.3.

Another highlight of the proposed hybrid approach with matching point distribution over a particle surface is the ability to use one and the same matrix while investigating scattering of different incident waves by the obstacle. Namely, it is possible to distribute DS inside the obstacle, compute matrix in (25) just once, and then construct pseudo-solutions to the overdetermined system of equations with different right hand parts $(\mathbf{E}_0^0 \cdot \hat{\tau}, \mathbf{E}_0^0 \cdot \hat{t}, \mathbf{H}_0^0 \cdot \hat{\tau}, \mathbf{H}_0^0 \cdot \hat{t})^T$. These right hand parts correspond to different excitations including plane waves propagating under different angles θ_0 or electrons with different impact parameters $\mathbf{b}$. It should be noted that generally it is not always possible to construct a DS set ensuring perfect results for all types of external excitations at once which is proved by the means of residual evaluation, but it is still a very important feature for conducting high performance estimates, especially for the problems in the layered medium which require more resources due to Sommerfeld integration.

3.3. Simulation results

In this section we would consider single prolate spheroid with semi-axes $a < b$ as particle. We would divide spheroid surface into the sectors of equal square and put a matching point P_l to the center of each

sector. Correspondingly, we would perform residual estimation at the B_l points distributed over sector borders.

Firstly, let us consider scattering problem in a homogeneous exterior domain D_0. Similar problems were previously solved many times within various DSM schemes, as well as within other techniques, which provides numerous opportunities to verify the new numerical algorithm. Usually, PW scattering problems are considered. However, it also appears possible to solve the scattering problem for other incident fields, one of them being EELS excitation (15). With latter being one of the recent advances within DSM, we would like to present a comparison of analytically computed EEL spectra (24) versus the one computed within hybrid DSM.

As analytical solution [14] is only available for spherical particles, we shall assume that particle with $a = b = 2$nm is deposited in the vacuum $\varepsilon_0 = \mu_0 = 1$ with center of the sphere coinciding with the origin of the Cartesian coordinate system. Here we shall also assume that our particle is made of either silver or gold. For excitation we shall consider an electron with $v = 50$keV and impact parameter $\mathbf{b}_x = 2.3$nm, $\mathbf{b}_y = 0$. This input allows to obtain EEL spectra presented in figure 1.

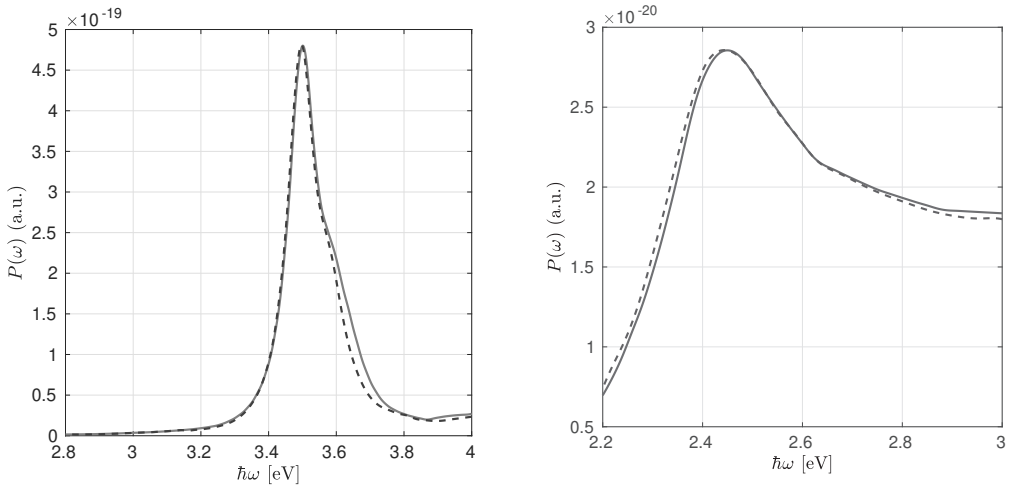

Figure 1. EEL spectra of the Ag (left) and Au (right) spherical particles with diameter $d = 4$nm located in the vacuum. Solid lines – analytic solution computed according to [14]. Dashed lines – DSM solution.

As we can see, both analytic and DSM results are in good agreement. From the point of physics, it is important that DSM allows to resolve plasmon resonance (PR) peak of the particle and study its characteristics, which is relevant to a wide range of plasmonic applications due to high sensitivity of PR to the material and shape of the particle. In the following we would mainly investigate the behaviour of peak resonance frequency $\hbar\omega_0$ (or wavelength λ_0). Here for Ag sphere $\hbar\omega_0 \sim 3.5$eV, while for Au sphere its value is around 2.45eV.

However, there are certain things to be commented on from the computational point of view. Most importantly, it is the behaviour of surface residual. Here an a posteriori error estimate gives residual values around 15% at best. This is due to the fact that scattering problem is solved in the near field with electron trajectory being very close to the boundary. For the same reason a relatively large number of matching points and discrete sources is required to perform computations. Here we employ $K = 225$ matching points and $N = 15$ points with Discrete Sources. Larger particles require significant increase of these values, however it is important that our aim is to specifically consider small obstacles. It should be also noted that decrease of the electron impact parameter $\mathbf{b}$ predictably leads to the exponential increase of the residual and, on the opposite, for the larger values of $\mathbf{b}$ residual values exponentially drop. The residual may also be significatly affected by the material parameters of the exterior domain and by the particle size which will be the case in section 4.5.

Figures similar to fig. 1 can be easily obtained for the SCS in plane wave scattering problem. We would omit them in this section as they are much more relevant to the section 4.5. Instead, here we would like to outline that in order to solve PW scattering by sphere in the far zone it is sufficient to

employ only $K = 49$ matching points and $N = 3$ points with Discrete Sources as opposed to the EELS problem. Residual estimate is then below 1%.

Secondly, we would like to consider PW scattering problem with the layered exterior domain composed of two homogeneos layers $D_{0,1}$ and infinite flat interface Σ between them. Keeping in mind that approach proposed in section 2.2 is justified for the small particles, let us intentionally attempt to investigate DSC of the larger spheroid with $a = 20$nm, $b = 200$nm under different angles θ_0 of incident plane wave. Here spheroid is elongated along the x axis and the distance between spheroid and substrate is 0.1nm. For simplicity let us assume that spheroid is transparent: $\varepsilon_T = 1.52, \mu_i = 1$. We would also assume that $\varepsilon_0 = \mu_0 = 1$, and that D_1 is made of silicon ($\varepsilon_1 = 4.15 - 0.047j, \mu_1 = 1$ at $\lambda = 532$nm). Corresponding results are presented in figure 2.

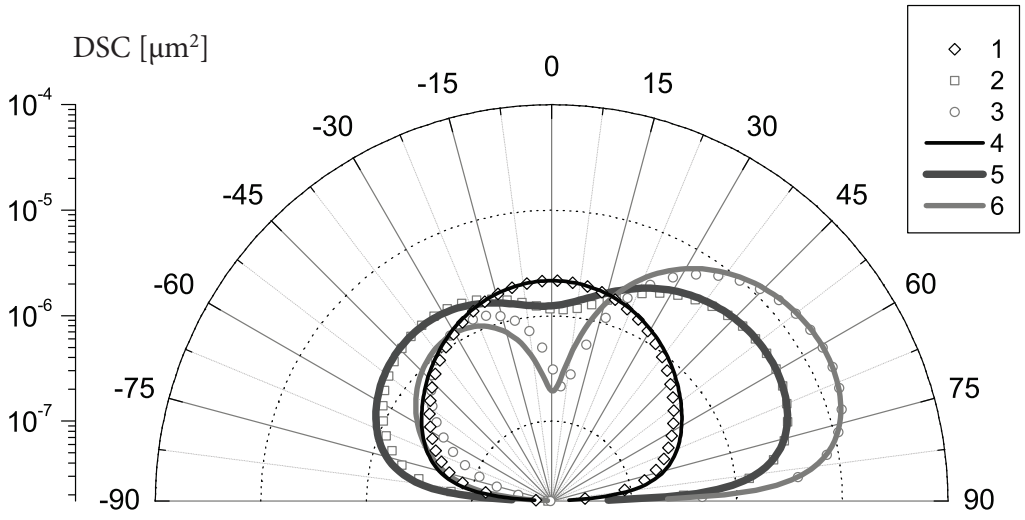

Figure 2. SCS for plane P-polarized wave scattering by a glass ($\varepsilon_T = 1.52$) spheroid deposited on a silicon substrate under different angles of incidence: $\theta_0 = 0$ (curves 1,4), $\theta_0 = \pi/6$ (curves 2,4) and $\theta_0 = \pi/3$ (curves 3,6). Symbolic lines – computations using general DSM approach. Solid lines – computations using the new hybrid DSM scheme.

Here we compare the results obtained with the proposed new scheme (curves 4–6) and with the long established general DSM scheme (curves 1–3). The important outcome is that usage of dipole sources on the particle axis still ensures acceptable results even for the particles which scale exceeds the theoretical estimate (7). Residual values here are around 13% at maximum, which occurs at $\theta_0 = \pi/3$. Therefore, the proposed approach can also be efficiently used to compute scattering by plane waves propagating under different angles of incidence using one and the same matrix as indicated in the previous section.

Now having established the proposed approach, let us proceed to the analysis of small plasmonic particles which requires further development of both mathematical model and computational algorithm.

4. NONLOCAL 3D SCATTERING PROBLEMS

4.1. Accounting for spatial dispersion in metals: new problem statement

Modern optic and photonic technologies require analysis of obstacles which size is comparable to the atomic scale. At the same time, when object size is reduced down to these scales, its real scattering properties begin to deviate from the ones predicted by classical electrodynamics. This deviation begins far before the obstacle scale reaches Angström limits – namely, differences in scattering properties are quite pronounced already at $a = 10$nm. These scales are still far too large to efficiently compute using quatum-based approaches. Besides, in the particle systems, even if the particle size is larger than 10nm, results of classic electrodynamics could still be inaccurate due to small (< 5nm) gaps between particles [15]. For this reason many attempts have been made to account for effects causing these deviations within Maxwell equations.

One of these effects is spatial dispersion of the particle material which is non-negligible at the considered scales. Spatial dispersion leads to the more complicated form of constitutive relations as opposed to the ones traditionally used in solving scattering problems [2]. From the point of physics, when we reduce the metal particle size to a scale smaller than electron mean free path, volume currents appear in the interior domain. Then internal electromagnetic field ceases to be purely transversal ($\mathbf{E}_T$) and obtains longitudinal ($\mathbf{E}_L$) component. Key thesis is that account for longitudinal waves actually allows to account for the spatial dispersion in metals. The main problem is that in order to appropriately describe the behaviour of longitudinal waves additional theoretical framework is required.

Among the latest developments on this topic the Generalized Nonlocal Optical Response (GNOR) theory has received our attention [16]. Its foundations lie in the Drude hydrodynamic theory (HDT) describing properties of electron gas in metals. Its findings can be briefly summarized as follows.

First of all, using GNOR results in the modification of one of the constitutive relations – Ohm law:

$$\left(\frac{\beta^2}{\omega^2 - j\gamma\omega} - \frac{D}{j\omega}\right) \nabla \left(\nabla \cdot \mathbf{J}(\mathbf{r},\omega)\right) + \mathbf{J}(\mathbf{r},\omega) = \sigma_d \mathbf{E}(\mathbf{r},\omega).$$

Here σ_d corresponds to Drude conductivity, γ – to Drude damping, $\beta^2 = (3/5)v_F^2$ – to Fermi velocity, D – to electron diffusion constant, and $\mathbf{J}$ is current density. Comparison with the traditional Ohm law $\mathbf{J}(\mathbf{r},\omega) = \sigma_d \mathbf{E}(\mathbf{r},\omega)$ allows to state that in its new form response of the material depends on the field distribution in some vicinity of current position instead of being dependent solely on the field value at $\mathbf{r}$. Today this behaviour is commonly known as nonlocal response, or nonlocal effect, and it is related to the spatial dispersion of the material [2]. In the following we would use notation Local Response Approximation (LRA) for the problems not accounting for nonlocal effect which were thoroughly investigated in the previous sections.

Secondly, within both HDT and GNOR it is possible to compute wave number of the longitudinal wave:

$$k_L^2 = \frac{\omega^2 - j\gamma\omega - \omega_p^2/\varepsilon_{core}}{\beta^2 + D(\gamma - j\omega)}. \tag{26}$$

Here ω_p corresponds to the plasma frequency of the metal and ε_{core} corresponds to the contribution from bound electrons and ions into dielectric permittivity.

And finally, account for the modified Ohm law leads to the new form of one of the Maxwell equations in the spatially dispersive interior domain D_i:

$$\mathrm{curl}\mathbf{H}_i(M) = jk\left(\varepsilon_T \mathbf{E}_i(M) + \xi^2 \mathrm{graddiv}\mathbf{E}_i(M)\right). \tag{27}$$

Here $\xi^2 = \varepsilon_{core}\left(\beta^2 + D(\gamma - j\omega)\right) / \left(\omega^2 - j\gamma\omega\right)$.

Therefore, in order to solve the scattering problem with account for spatial dispersion effects it is required to consider total electric field as $\mathbf{E}_i = \mathbf{E}_T + \mathbf{E}_L$ and to replace the equation (13a) with (27). However, now there is a new unknown field $\mathbf{E}_L$ in the problem (13), and it is also required to impose an additional boundary condition in order to ensure the existence of unique solution. In this paper we would follow an assumption that $\mathbf{J} \cdot \hat{\mathbf{n}}_P = 0$ which leads to [16]

$$\hat{\mathbf{n}}_P \cdot \varepsilon_{core} \mathbf{E}_i(P) = \hat{\mathbf{n}}_P \cdot \varepsilon_0 \mathbf{E}_0(P), \quad P \in \partial D_i. \tag{28}$$

This expression should also be added to the conditions on the tangential components (13g) and (13h) in problem statement.

4.2. Features of the longitudinal waves

It is necessary to address one certain feature of the longitudinal waves before proceeding to the development of the appropriate DSM model. In order to do so let us consider specific materials: silver with parameters $\hbar\omega_p = 8.99\text{eV}$, $\hbar\gamma = 0.025\text{eV}$, $v_F = 1.39 \cdot 10^6$ ms^{-1}, $D = 3.61 \cdot 10^{-4}$ m^{2}s^{-1} and gold with $\hbar\omega_p = 9.02\text{eV}$, $\hbar\gamma = 0.071\text{eV}$, $v_F = 1.39 \cdot 10^6$ ms^{-1}, $D = 1.90 \cdot 10^{-4}$ m^{2}s^{-1} [16]. Our aim is to investigate the behaviour of longitudinal wave number k_L. To do this we would first have to determine the

value of ε_{core}. This can be achieved via Drude expression for the dielectric permittivity of the transversal waves ε_T, which in turn can be measured experimentally [17]:

$$\varepsilon_{core} = \varepsilon_T + j\frac{\omega_p^2}{\omega(\omega - j\gamma)}$$

Then using expression (26) we could obtain values of k_L as presented on fig. 3 (HDT values are computed with $D = 0$).

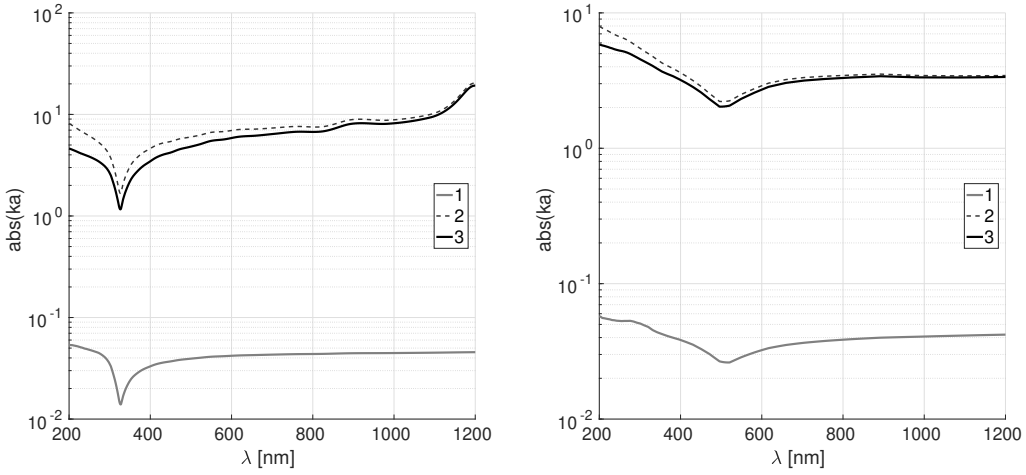

Figure 3. Absolute values of the dimensionless wave numbers in case of silver (left) and gold (right) materials. Curves 1 – wave number k_T of the transversal wave. Curves 2 – wave number k_L of the longitudinal wave within HDT. Curves denoted as 3 – wave number of the longitudinal wave according to GNOR.

We can clearly see that longitudinal wave numbers (curves 2 and 3) exceed transversal ones (curves 1) by the order of magnitude leading to high oscillating fields. This feature could restrict or make less efficient appication of many direct numerical approaches like FEM or FDTD to the solution of nonlocal scattering problem. We should also emphasize the fact that while transversal field is divergence-free ($\mathrm{div}\mathbf{E}_T = 0$), longitudinal field is actually curl-free ($\mathrm{curl}\mathbf{E}_L = 0$) [16]. For this reason $\mathbf{H}$ field is not affected by the longitudinal waves in GNOR approximation as follows from (13b).

4.3. Discrete Sources for the longitudinal fields

In order to apply the DSM to solve nonlocal problem statement (27,13b-13f,28,13g-13l) it is necessary to construct discrete sources that would approximate longitudinal waves. Here we would use the fact that modified Maxwell equation (27) can be rewritten in the form of two Helmholtz equations separately describing transversal and longitudinal fields:

$$\left(\nabla^2 + k_L^2\right)\mathrm{div}\mathbf{E}(\mathbf{r},\omega) = 0, \quad \left(\nabla^2 + k_T^2\right)\mathrm{curl}\mathbf{E}(\mathbf{r},\omega) = 0. \tag{29}$$

Indeed, we can arrive at these equations by substituting $\mathbf{H}$ from (13b) into (27) and then applying $\mathrm{curlcurl}\mathbf{E} = \mathrm{graddiv}\mathbf{E} - \nabla^2\mathbf{E}$ to the resulting expression. In particular, to arrive to the Helmholtz equation for the longitudinal waves, it is necessary to exclude 'graddiv' term from the obtained equation and apply the divergence operator, while to obtain expression for transversal waves 'curlcurl' term should be excluded and curl operator should be applied.

Based on the first equation in (29) we can obtain required expressions for the longitudinal Discrete Sources. Taking into account $\mathrm{curl}\mathbf{E}_L = 0$ and concept of the DSM hybrid scheme, let us write down

$$\mathbf{E}_{L,j_0}(M, M_n) = \mathrm{grad}\left(j_0(k_L R_{MM_n})\right), \tag{30}$$

$$\mathbf{E}_{L,\cos\phi}(M, M_n) = \mathrm{grad}\left(j_1(k_L R_{MM_n})\sin\Theta\cos\phi\right), \tag{31}$$

$$\mathbf{E}_{L,\sin\phi}(M, M_n) = \mathrm{grad}\left(j_1(k_L R_{MM_n})\sin\Theta\sin\phi\right), \tag{32}$$

where Θ and ϕ are spherical coordinates of observation point M related to the point M_n. Then, assuming that DS are located in the same points $\{M_n\}_{n=1}^N$ as DS for transversal and exterior fields, approximate solution for the longitudinal field takes the form:

$$\mathbf{E}_L^N(M) = \sum_{n=1}^{N} \sum_{\alpha=j_0,\cos\phi,\sin\phi} p_{\alpha,n}^L \mathbf{E}_{L,\alpha}(M, M_n), \tag{33}$$

Now to compute the internal field expression (33) has to be used along with (16), $\mathbf{E}_i$ being replaced by $\mathbf{E}_T$ in the latter.

4.4. Numerical algorithm

New problem statement with the additional boundary condition and longitudinal discrete sources leads to the introduction of new equation into (25):

$$\varepsilon_{core}\left(\mathbf{E}_T^N(P_l) + \mathbf{E}_L^N(P_l)\right)\cdot\hat{\mathbf{n}}_{P_l} = \varepsilon_0\left(\mathbf{E}_0^{S,N}(P_l) + \mathbf{E}_0^0(P_l)\right)\cdot\hat{\mathbf{n}}_{P_l} \tag{34}$$

Consequently, number of matching points should now satisfy $K > 15N$. These modifications do not result in any principal algorithm changes, however due to the high oscillating fields it might be necessary to increase the amount of longitudinal DS and matching points, correspondingly. It is important to note here that spatial dispersion effects within the considered GNOR approach do not affect the exterior domain, and corresponding solution can be constructed precisely following (18). The same stands for the scattering characteristics.

Most notably, the proposed DSM scheme and its computational algorithm can be efficiently applied to solve problems featuring spatial dispersion as it is initially designed for small particle analysis (see section 2.2).

4.5. Simulation results and discussion

It is important to verify the proposed approach with account for nonlocal reponse. It is reasonable to begin with comparison to the analytic solutions available both in LRA and GNOR for spherical particles located in the homogeneous exterior domain D_0.

First of all, let us consider silver sphere irradiated by a plane P-polarized wave ($\theta_0 = 0$) and let us vary its diameter $d = 2a$. In this section we would compute SCS according to (23). Corresponding results are presented in the left part of figure 4.

There are several important conclusions to be made according to the presented data. Let us begin with the computational ones: it is obvious that the proposed DSM approach is able to accurately simulate scattering properties of small plasmonic spheres both within LRA and GNOR techniques as shown by the coincidence of symbolic and solid curves 1–6. Here for each sphere $K = 289$ matching points were used along with $N = 7$ points with the so-called local discrete sources (16,18) and with $N = 15$ points with the nonlocal DS (33) ensuring residual values to be far below 1% for particles of all sizes. The same results can be obtained with lower amount of both K and N: even for the values of $N = 3$ and $K = 49$ the problem is solved and the residual is not larger than 3%. It should be noted that generally it is necessary to choose more nonlocal than local DS according to the features of the longitudinal waves described in section 4.2.

Next conclusion is the importance of account for nonlocal effects as there appear to be substantial differences between LRA and GNOR computations. These differences result in the intensity drop of the resonant peak by the order of magnitude and, most importantly, in the blue-shift of the resonant wavelength λ. For larger particles these differences are less pronounced, while for the smaller particles the difference becomes more clear. Namely, $\lambda_{GNOR} = 347$nm for a $d = 3$nm particle, and $\lambda_{GNOR} = 351.5$nm for the $d = 9$nm particle. At the same time the $\lambda_{LRA} = 355$nm for particles of all sizes. So the account for nonlocal effect (27,13b-13f,28,13g-13l) allows to resolve peak shift which is not present in the computations using the traditional problem statement (13).

The impact of nonlocal effect has already been confirmed experimentally. In particular, EELS instruments have proved to be convenient to measure response of single silver particle embedded in

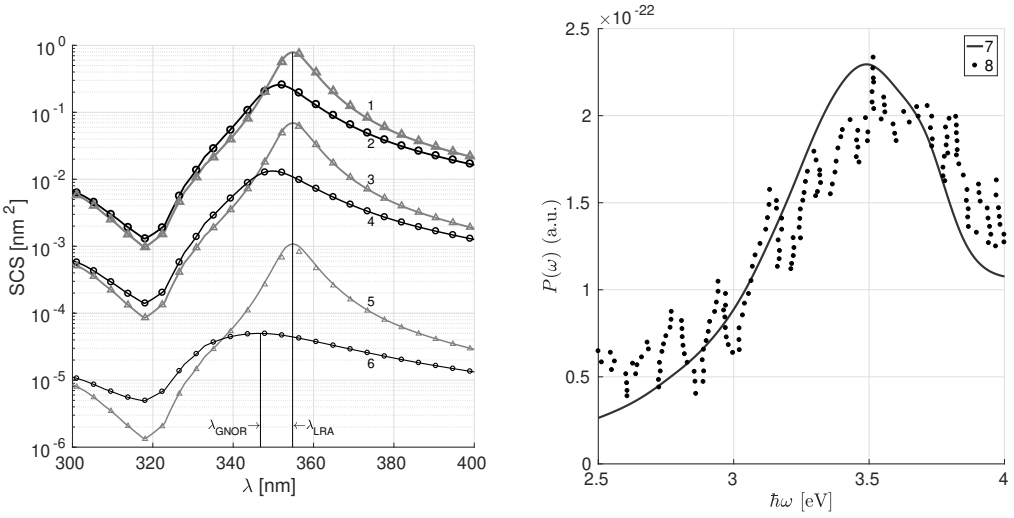

Figure 4. *To the left*: SCS for the Ag spheres computed analytically (solid lines) and using DSM (symbolic lines) in local response approximation (grey) and with account for nonlocal effect via GNOR (black) with variable diameter d (curves 1, 2: $d = 9$nm, curves 3, 4: $d = 6$nm, curves 5, 6: $d = 3$nm). $\lambda_{GNOR,LRA}$ denote corresponding resonant frequencies for the $d = 3$nm. *To the right*: EEL spectra for the Ag sphere with $d = 2$nm embedded in silica. Solid line 7 – DSM results. Black dots 8 – experimental measurements data according to [18].

silica [18]. These results can be reproduced within DSM by substituting frequency-dependent material parameters of silica instead of exterior domain parameters ε_0, μ_0. Let us perform these computations as our second step.

Using previously defined values for the K and N, let us consider silver sphere with diameter $d = 2$nm embedded in silica and compute EEL spectra within DSM. Corresponding results are presented in the right part of figure 4 with black dots referring to the experimental data and with solid curve referring to the DSM computations. Here electron excitation parameters are $v = 60$keV and $|\mathbf{b}| = 2.25$nm. Most notably, the introduction of silica exterior along with the reduction of the particle size resulted in the surface residual values to be around 0.5-1%.

Thirdly, let us pay closer attention to the resonant frequency behaviour. Let us vary the diameter d of the silver particle embedded in silica and compute resonant $\hbar\omega_0$ values maintaining the amount of matching points and discrete sources. Relevant results are presented on the left part of figure 5. The outcome is that nonlocal effect impact results in the experimentally observed shift of the resonant peak from ~ 3.1eV in the local response approximation to ~ 3.5 within GNOR for the particle with $d = 2$nm almost coinciding with the resonant frequency value for silver in vacuum. It can be seen that resonance peak shifts are more pronounced in the medium, that their effect is definitely non-negligible in plasmonic applications, and that it is possible to perform relevant simulations with the Discrete Sources Method.

Finally, let us consider a plane wave scattering problem with account for nonlocal effect for silver oblate spheroids with $a > b$ deposited on a substrate. In the case of oblate obstacles it is necessary to move discrete sources positions into the complex plane following the procedure that is well-described in the previous DSM research [5, 8]. In order to investigate the behaviour of size-dependent plasmon resonance peaks let us introduce the equivolume diameter of the oblate spheroid $d^3 = 8a^2b$ along with aspect ratio $r = a/b$. Let us fix $d = 10$nm and vary r. Corresponding results are presented on the right part of figure 5.

Substrate impact can be clearly seen: the red-shift of the resonance peak in case of silver substrate (curves 8–10) is even more pronounced than for the particle on the transparent substrate (curves 5–7), where it was caused solely by the particle squeezing. Additionally, in the case of silver substrate a second resonant peak emerges and the scattering intensity is almost doubled. Here residual estimate does not exceed 2%.

To conclude the current section, it should be also noted that proposed numerical scheme has also been extended to investigate particle dimers [10].

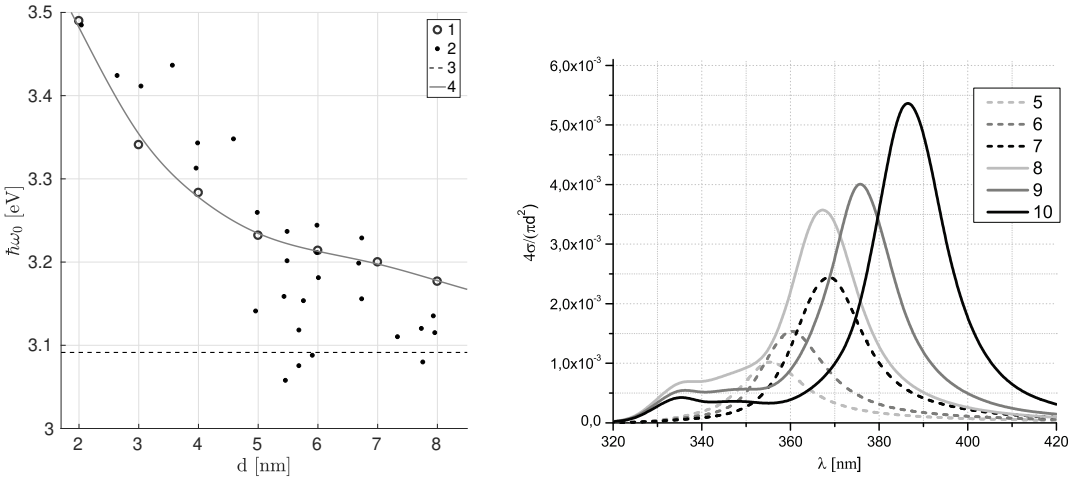

Figure 5. *To the left*: dependence of the plasmon resonance frequency $\hbar\omega_0$ on the diameter d of Ag sphere embedded in silica. Circles 1 – DSM simulations, black dots 2 – experimentally measured values according to [18], dashed line 3 – constant LRA value of the silver plasmon resonance frequency in silica, solid curve 4 – spline fit to the DSM data. *To the right*: SCS for the Ag oblate spheroid with equivolume diameter $d = 10$nm and aspect ratio r deposited on the substrate. Curves 5, 8 – spherical particle with $r = 1.0$, curves 6, 9 – oblate spheroid with $r = 1.2$, curves 7, 10 – particle with $r = 1.5$. Dashed curves– particles deposited on a transparent substrate ($n_1 = 1.52$), solid curves – particles deposited on a silver substrate.

5. CONCLUSION

New Discrete Sources Method-based mathematical models for both plane wave scattering and electron energy loss were proposed, developed and verified. Account for the nonlocal effect allowing to study influence of material spatial dispersion on the experimentally measurable properties of the obstacle was incorporated into the models. Using well-developed theoretical framework of the DSM it has been shown that for the problems featuring small-scaled axisymmetric particles (< 10nm) it is sufficient to employ dipole discrete sources on the axis along with the distribution of matching points all over the particle surface in order to solve the problem. Scattering problems were solved for single particles such as spheres, prolate and oblate spheroids deposited either in homogeneous exterior domain or in the layered medium with two homogeneous layers and plane infinite interface between them. Obtained results form a foundation for implementing new efficient computational schemes and algorithms for accurate analysis of nanostructures relevant in modern nanoplasmonic and biophotonic applications, including such structures as groups of particles (dimers, trimers and clusters).

Acknowledgments. This work was financially supported by the Russian Foundation of Basic Research: grant 20-01-00558-A.

REFERENCES

1. S. A. Maier, *Plasmonics: Fundamentals and Applications* (Springer, 2007).
2. L. D. Landau and E. M. Lifshitz, *Electrodynamics of Continuous Media* (Pergamon Press Ltd, 1984).
3. F. J. G. de Abajo, "Optical excitations in electron microscopy,"Reviews of Modern Physics **82** (1), 209–275 (2010).
4. V. D. Kupradze, "O priblizhennom reshenii zadach matematicheskoy fiziki,"Russian Math. Surveys **22** (2), 58–108 (1967) [in Russian].
5. Yu. A. Eremin and A. G. Sveshnikov, *Metod diskretnikh istochnikov v zadachakh electromagnitnoy difraktsii* (Izdatelstvo Moskovskogo Universiteta, 1992) [in Russian].
6. A. S. Il'inskii and A. G. Sveshnikov, *Chetyre lektsii po chislennim metodam v teorii difraktsii* (Izdatelstvo Leningradskogo Gosudarstevnnogo Universiteta imeni Zdanova, 1972) [in Russian].
7. A. S. Il'inskii, V. V. Kravtsov and A. G. Sveshnikov, *Matematicheskie modeli elektrodinamiki* (Vysshaya shkola, 1991) [in Russian].
8. A. Doicu, Y. Eremin and T. Wriedt, *Acoustic and electromagnetic scattering analysis using Discrete Sources* (Academic Press, 2000).

9. Yu. A. Eremin and I. V. Lopushenko, "A Hybrid Scheme of the Discrete Sources Method for Analyzing Boundary Value Problems of Nano-Optics,"Moscow Univ. Comput. Math. Cynern. **40** (1), 1–9 (2016).
10. Yu. A. Eremin and I. V. Lopushenko, "An Analysis of the Quantum Effect of Nonlocality in Plasmonics Using the Discrete Sources Method,"Moscow University Physics Bulletin **74** (6), 570–576 (2019).
11. V. I. Dmitriev and E. V. Zakharov, *Metod integral'nykh uravneniy v vychislitelnoy elektrodinamike* (MAKS Press, 2008) [in Russian].
12. L. F. Shampine, "Vectorized adaptive quadrature in MATLAB,"Journal of Computational and Applied Mathematics **211** (2), 131–140 (2008).
13. M. Mori and M. Sugihara "The double-exponential transformation in numerical analysis,"Journal of Computational and Applied Mathematics **127** (1-2), 287–296 (2001).
14. F. J. G. de Abajo, "Relativistic energy loss and induced photon emission in the interaction of a dielectric sphere with an external electron beam,"Physical Review B **59** (4), 3095–3107 (1999).
15. T. V. Teperik et al, "Quantum effects and nonlocality in strongly coupled plasmonic nanowire dimers,"Optics Express **21** (22), 27306 (2013).
16. S. Raza, Ph.d. diss., Department of Photonics Engineering and the Center for Electron Nanoscopy, Technical University of Denmark, Denmark (2014).
17. P. B. Johnson and R. W. Christy, "Optical constants of the noble metals,"Phys Rev. B **6** , 4370–4379 (1972).
18. A. Campos et al, "Plasmonic quantum size effects in silver nanoparticles are dominated by interfaces and local environments,"Nature Physics **15** (3), 275–280 (2018).